

# Synthesis and Electrochromic Properties of Conducting Polymers Based on Highly Planar 2,7-Disubstituted Xanthene Derivatives

Kamila Olech,<sup>[a]</sup> Ramona Gutkowski,<sup>[b]</sup> Volodymyr Kuznetsov,<sup>[b]</sup> Szczepan Roszak,<sup>[a]</sup> Jadwiga Sołoducho,<sup>\*[a]</sup> and Wolfgang Schuhmann<sup>\*[b]</sup>

On the basis of preliminary DFT calculations, p-type semiconducting polymers based on 2,7-substituted xanthene building blocks that show a high degree of planarity were designed. The synthesis, electrochemical characterization, and theoretical modeling of 2,7-bis(thiophen-2-yl)-9,9-dimethylxanthene (1) and 2,7-bis(3-hexylthiophen-2-yl)-9,9-dimethylxanthene (2) is described. The synthetic procedure is based on the incorporation of thiophene rings by means of Pd-catalyzed cross-cou-

pling reactions, which lead to monomers 1 and 2. Copolymers P1 and P2 obtained by means of anodic polymerization have been characterized by spectroscopic and electrochemical methods. Electrochromism was observed for both polymers. The experimental data supported by density functional theory modeling explain the influence of alkyl chain substitution on the properties of the investigated copolymers.

## Introduction

Semiconducting organic materials possess broad application potentials in layered, microscopic electronics: for example, as light-emitting diodes, photovoltaic devices, and sensors.<sup>[1]</sup> In this context, electronically conducting polymers that demonstrate high conductivity upon doping are of particular interest. Chemical or electrochemical doping leads to the formation of solitons, polarons, or bipolarons, which are delocalized over the polymer molecules and act as charge carriers.<sup>[2]</sup> The optoelectronic properties, processability, and functionality of organic semiconducting materials are readily tunable by changing their composition and molecular weight.<sup>[3]</sup>

A convenient approach to obtain organic materials with suitable bandgaps is to design and synthesize donor–acceptor (DA) type macromolecules. The alternate incorporation of electron-rich and electron-deficient units into the molecular backbone decreases the HOMO–LUMO energy gap owing to the expansion of the delocalized  $\pi$ -electron orbital.<sup>[4]</sup> The electronic properties are strongly influenced by the chemical composition of related copolymers. The steric factors of polymer matrix formation and matrix defects also contribute considerably to

those properties. Thus, the development of synthesis methods as well as the selection of suitable building blocks are prioritized approaches in the design of low-bandgap polymer composites.

Despite the fact that many heteroaromatic compounds have been explored, comparatively little attention has been devoted to xanthene derivatives; mainly materials based on rhodamine,<sup>[5]</sup> spiroxanthene,<sup>[6]</sup> and dibenzoxanthene<sup>[7]</sup> have been investigated. The first report on xanthene-based polymers was published in 2010 by Morisaki et al.,<sup>[8]</sup> who described 4,5-substituted xanthene oligomers as highly thermally stable, layered, and hole-transporting materials. More recently, 9,9-dimethylxanthene was proposed as a bridge for perylene multichromophore covalent dimers.<sup>[9]</sup> To the best of our knowledge, 2,7-heterocycle-substituted xanthene derivatives and their electropolymerization have not yet been reported.

In this study, we present the synthesis, electrochemically induced polymerization, and characterization of 2,7-substituted xanthene derivatives, which show a high degree of planarity that can significantly affect the electrical and optical properties of related oligomers or polymers. Specifically, we investigated 2,7-bis(thiophen-2-yl)-9,9-dimethylxanthene (1) and its alkylated analogue (2) as precursors for new electrochromic semiconducting materials. The initial evaluation of the physicochemical properties of the corresponding polymers films P1 and P2 were performed by cyclic voltammetry, electrochemical impedance spectroscopy, and spectroelectrochemical measurements. Experimental results were supported by theoretical modeling based on density functional theory (DFT). The role of the alkyl chain with respect to the optoelectronic properties of electronically conducting xanthene polymers is discussed on the basis of both the calculated and atomic force microscopy (AFM) structure visualization.

[a] K. Olech, Prof. Dr. S. Roszak, Prof. Dr. J. Sołoducho  
Faculty of Chemistry  
Wrocław University of Technology  
Wybrzeże Wyspiańskiego 27  
50-370 Wrocław, Poland  
E-mail: jadwiga.soloducho@pwr.edu.pl

[b] R. Gutkowski, Dr. V. Kuznetsov, Prof. Dr. W. Schuhmann  
Analytical Chemistry–Center for Electrochemical Sciences (CES)  
Ruhr-Universität Bochum, Universitätsstrasse 150  
44780 Bochum (Germany)  
E-mail: wolfgang.schuhmann@rub.de

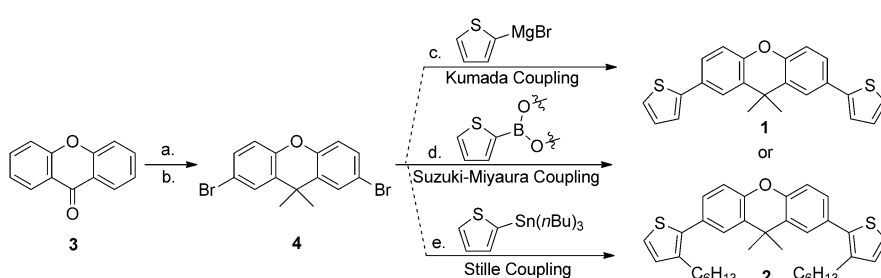
Supporting information for this article is available on the WWW under <http://dx.doi.org/10.1002/cplu.201402349>.

## Results and Discussion

### Synthesis of 1 and 2

The synthesis of monomers **1** and **2** is presented in Scheme 1. A variety of condensation reactions was investigated to symmetrically substitute the xantheno moiety with thiophene rings. Kumada-type coupling was found to be the least efficient as it uses air- and moisture-sensitive Grignard reagents, which were unstable over the reaction time. Thus no reaction progress was observed after one day according to thin-layer chromatography (TLC), whereas in the reaction mixture a high concentration of unreacted educts was detected. The long-time synthesis with organotin species according to the Stille protocol gave about 45% of crude products with impurities that were difficult to separate chromatographically. The latter were characterized by a retention factor close to that of the xantheno derivative (**1**).

The Suzuki–Miyaura reaction in mixed aqueous/ethoxyethanol solvent (1:9), reported previously for the coupling of thiophene with different arenes,<sup>[10]</sup> was found to be the most successful synthesis pathway when considering both efficiency and reaction time. An additional advantage is the nontoxicity of byproducts.<sup>[11]</sup>



**Scheme 1.** Synthesis of 2,7-disubstituted xantheno derivatives **1** and **2**. a)  $\text{Me}_3\text{Al}$ ,  $\text{PhCH}_3$ ; b)  $\text{Br}_2$ ,  $(\text{CH}_3\text{CO})_2\text{O}$ ,  $\text{CH}_3\text{COOH}$ ; c)  $[\text{Ni}(\text{dppp})\text{Cl}_2]$  ( $\text{dpppp} = 1,3\text{-bis}(\text{diphenylphosphino})\text{propane}$ ),  $\text{Et}_2\text{O}$ , 72 h; d) 0.4 mol %  $[\text{Pd}(\text{PPh}_3)_4]$ ,  $\text{K}_2\text{CO}_3$ ,  $\text{EtO}(\text{CH}_2)_2\text{OH}/\text{H}_2\text{O}$  (9:1), 24–48 h; and e)  $[\text{PdCl}_2(\text{PPh}_3)_2]$ , tetrahydrofuran (THF), 48 h.

Compounds **1** and **2** were obtained with 42 and 31% yields, respectively. They exhibit good solubility in common organic solvents such as chloroform and acetonitrile. The possibility of their synthesis by a convenient solution-processable technique or thermal evaporation at room temperature can be considered an advantage over inorganic-based semiconductor devices.<sup>[1b]</sup>

### Electrochemical properties

Cyclic voltammetry (CV) of solutions of monomers **1** and **2** in acetonitrile (both 0.50 mM) was carried out to create thin films of the corresponding copolymers **P1** and **P2**. As can be seen from the voltammograms, both synthesized monomers are electroactive (Figure 1). The oxidation potential is lower for thiophene than the 3-hexylthiophene ring and is 1.29 and 1.34 V for monomers **1** and **2**, respectively. This redox process is associated with the monoelectronic oxidation of the monomers to the corresponding radical cations.<sup>[12]</sup> The appearance of new oxidation peaks at 0.75 (in the case of **P1**) and 1.00 V (in the case of **P2**) after repetitive anodic scans clearly indicates the formation of electroactive oligomer films on the electrode surfaces. The slow charge transfer within the film and/or at the interfaces is illustrated by the broadening of the redox waves.<sup>[13]</sup> The lower intensity of the cathodic peak at 1.18 V suggests the consumption of radical cations during the polymerization reaction. Hence the increase in polymer thickness on the Pt electrode after each cycle is seen as an increase of the peak current. The redox conversion at about 0.1 V for **P1** in both the anodic and cathodic half-scans (Figure 1) indicates the formation of a quasi-reversi-

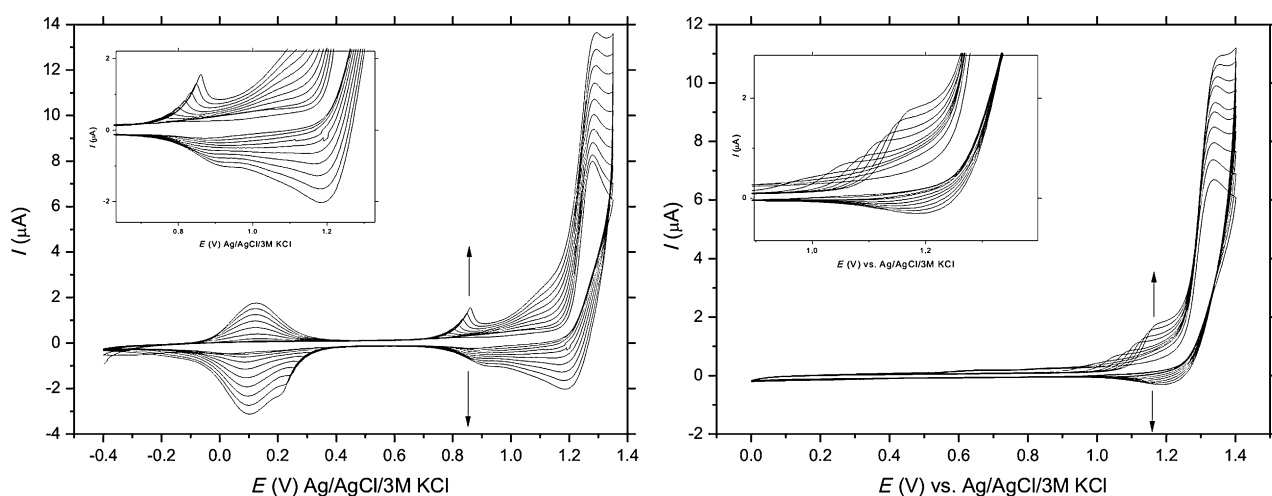


**Figure 1.** Cyclic voltammograms of the electrochemically induced polymerization of **1** (left) and **2** (right) in 0.1 M  $\text{Bu}_4\text{NPF}_6/\text{MeCN}$  with a scan rate of  $50 \text{ mVs}^{-1}$ . Monomer concentration was 0.50 mM. The potential was referenced against the  $\text{Ag}/\text{AgCl}/3 \text{ M KCl}$  electrode.

ble redox system during polymer deposition. The formation of **P1** and **P2** was confirmed by an optically visible green layer on the Pt surface.

The deposited films were additionally characterized by means of electrochemical impedance spectroscopy (EIS) in the presence of  $[\text{Fe}(\text{CN})_6]^{3-/4-}$  as a redox couple ( $c = 5 \text{ mM}$ ). Impedance spectra were acquired in a frequency range from 60 kHz to 0.01 Hz with an alternating current (ac) perturbation amplitude of  $10 \text{ mV}_{\text{rms}}$  at a constant direct current (dc) potential of  $+210 \text{ mV}$  versus the  $\text{Ag}/\text{AgCl}/3 \text{ M KCl}$  reference electrode. The film grown on the Pt electrode hinders the redox conversion of  $[\text{Fe}(\text{CN})_6]^{3-/4-}$ , which can be seen by a drastic increase in the charge-transfer resistance  $R_{\text{ct}}$ . The  $R_{\text{ct}}$  of **P2** is  $9.28 \text{ M}\Omega$  as determined from the diameter of the semicircle of the Nyquist ( $Z''$  versus  $Z'$ ) plot, in which  $Z'$  and  $Z''$  are real and imaginary parts of the impedance, respectively (Figure 2).

Compound **P1** shows a much higher  $R_{\text{ct}}$  than **P2**. This is surprising, because the thickness of the **P1** film (60–90 nm) is considerably smaller than that of the **P2** film (150–250 nm) as determined by AFM (see below). This effect could be attributed to the fact that the multilayer film of **P2** is most likely more porous owing to the presence of  $n$ -hexyl chains in the polymer backbone, which increase the distance between molecules. Therefore, charges from the electrolyte are better dispersed within the redox-active polymer

material. Since the charge percolation through the polymer matrix generally dictates operational characteristics of the deposited microstructure, it can explain the lower  $R_{\text{ct}}$  of **P2**.<sup>[14]</sup>

The stability of the obtained films was investigated by a sequential doping/dedoping process in monomer-free electrolyte using cyclic voltammetry at a scan rate of  $300 \text{ mV s}^{-1}$  in the potential range between  $-0.40$  and  $+1.35 \text{ V}$  and  $0.0$  and  $+1.40 \text{ V}$  for **P1** and **P2**, respectively. The height of the oxidation peaks decreases by approximately 50% after 25 voltammetric cycles for **P1** and after 55 cycles for **P2**. The higher stability of **P2** might be a consequence of the lower solubility owing to the likely higher molecular weight of the formed polymer chains. The bandgap as well as oxidation and reduction properties for the obtained polymers are given in Table 1.

**Table 1.** Calculated and experimental ionization energies ( $\epsilon_{\text{HOMO}}$ ,  $\text{IP}_{\text{ver}}$ ,  $\text{IP}_{\text{ad}}$ ), calculated and experimental electron affinity ( $\epsilon_{\text{LUMO}}$ ,  $\text{EA}_{\text{exp}}$ , cyclic voltammetry), calculated singlet and triplet electronic excited states ( $\Delta E_{\text{excited}}$ ), and corresponding experimental (UV/Vis and cyclic voltammetry) energy gap ( $\Delta E_{\text{HOMO/LUMO}}$ ) between valence and conduction bands for **P1** and **P2**. All energies are in eV.

	$n$	1	2	3	4	5	Monomer	Polymer
		Theoretical					Experimental	
<b>P1</b>	$\epsilon_{\text{HOMO}}$	-5.42	-5.07	-5.03	-5.02	-5.01	-	-5.47 <sup>[a]</sup>
	$\text{IP}_{\text{ver}}$	6.66	6.02	5.77	5.63	5.53	5.95 <sup>[a]</sup>	-5.47 <sup>[a]</sup>
	$\text{IP}_{\text{ad}}$	6.51	5.89	5.68	5.56	5.48	5.95 <sup>[a]</sup>	-5.47 <sup>[a]</sup>
	$\epsilon_{\text{LUMO}}$	-1.25	-1.83	-1.89	-1.92	-1.94	-	-2.77 <sup>[a]</sup>
	$\Delta E_{\text{HOMO/LUMO}}$	4.17	3.24	3.13	3.10	3.07	-	2.70 <sup>[a]</sup>
	$\Delta E_{\text{excited}}$ singlet	3.73	2.89	-	-	-	3.64 <sup>[b]</sup>	2.67 <sup>[b]</sup>
	$\Delta E_{\text{excited}}$ triplet	2.69	1.89	-	-	-	3.64 <sup>[b]</sup>	2.67 <sup>[b]</sup>
<b>P2</b>	$\epsilon_{\text{HOMO}}$	-5.53	-5.15	-5.11	-5.08	-5.08	-	-5.59 <sup>[a]</sup>
	$\text{IP}_{\text{ver}}$	6.70	6.08	5.82	5.67	5.58	6.00 <sup>[a]</sup>	-5.59 <sup>[a]</sup>
	$\text{IP}_{\text{ad}}$	6.49	5.89	5.73	5.60	5.64	6.00 <sup>[a]</sup>	-5.59 <sup>[a]</sup>
	$\epsilon_{\text{LUMO}}$	-0.93	-1.47	-1.52	-1.54	-1.56	-	-2.78 <sup>[a]</sup>
	$\Delta E_{\text{HOMO/LUMO}}$	4.59	3.67	3.59	3.54	3.52	-	2.81 <sup>[a]</sup>
	$\Delta E_{\text{excited}}$ singlet	4.06	3.27	-	-	-	3.83 <sup>[b]</sup>	2.78 <sup>[b]</sup>
	$\Delta E_{\text{excited}}$ triplet	3.04	3.03	-	-	-	3.83 <sup>[b]</sup>	2.78 <sup>[b]</sup>

[a] Experimental electrochemical. [b] Experimental UV/Vis spectroscopy.

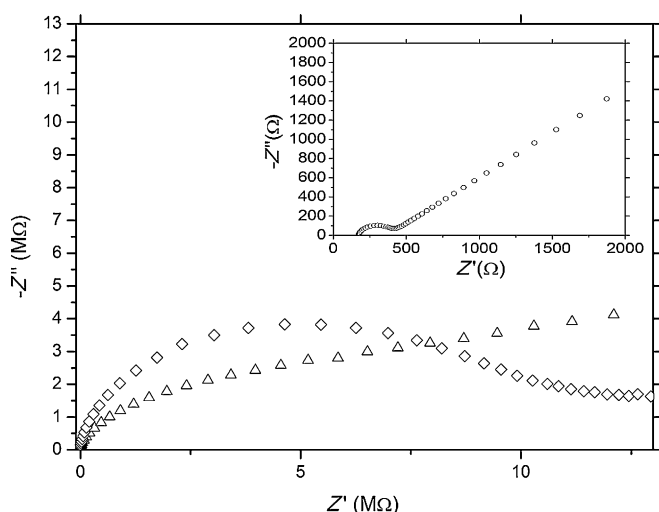


**Figure 2.** Nyquist plots of a bare Pt electrode (inset;  $\circ$ ) and after electrochemically induced polymerization of **1** ( $\Delta$ ) and **2** ( $\diamond$ ). EIS was recorded in the presence of  $5 \text{ mM } [\text{Fe}(\text{CN})_6]^{3-/4-}$  at  $+210 \text{ mV}$  versus  $\text{Ag}/\text{AgCl}/3 \text{ M KCl}$ ; perturbation amplitude:  $10 \text{ mV}_{\text{rms}}$  and frequency range:  $60 \text{ kHz}$  to  $0.01 \text{ Hz}$ .

The energy gaps of **P1** and **P2** deposited on a platinum electrode were derived from cyclic voltammetry measurements recorded in acetonitrile that contained  $0.1 \text{ M Bu}_4\text{NPF}_6$  at a scan rate of  $100 \text{ mV s}^{-1}$  (Figure 3). The distance between the irreversible oxidation and reduction potentials, which are correlated with the HOMO and LUMO energies, respectively,<sup>[15]</sup> are  $2.70 \text{ eV}$  for **P1** and  $2.81 \text{ eV}$  for **P2**.

### Spectroelectrochemical properties of polymers

The chemical changes that occur in the polymer films during the oxidative doping process were investigated by means of UV/Vis spectroelectrochemistry. In the negative potential range an absorption band with a maximum at  $318 \text{ nm}$  was observed for **P1** (Figure 4). For **P2** two absorption bands were recorded, which can be related to oligomers with significantly different chain lengths. The first band is close to the monomer absorption band and corresponds to short oligomers, whereas the second less-intense band at  $365 \text{ nm}$  is caused by longer polymer chains (Figure 4).

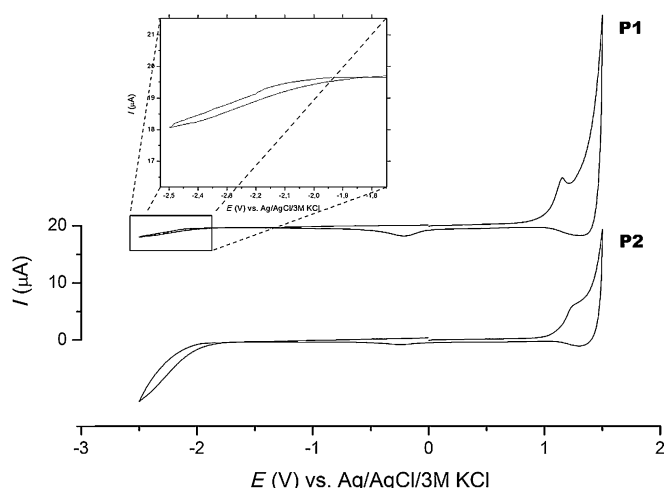


**Figure 3.** The electrochemical doping process of polymer **P1** and **P2** in 0.1 M  $\text{Bu}_4\text{NPF}_6/\text{MeCN}$  at a scan rate of  $100 \text{ mVs}^{-1}$ .

These absorption bands characterize the neutral, dedoped state, which corresponds to the  $\pi\text{-}\pi^*$  electron transition from the valance band to the conduction band.<sup>[16]</sup> Oxidation of the polymers led to the appearance of a new broad absorption band while simultaneously decreasing the intensity of the bands at lower wavelengths. The bands in the range of 500–800 nm can be attributed to the polaron generated during electrochemical doping.<sup>[17]</sup> Well-defined isosbestic points at 443 nm for **P1** and at 434 nm for **P2** reflect the transition of an insulating state into a conducting one. These transformations during oxidation were additionally evidenced by the polymer color change. A change in color from yellow (reduced form) to green and blue (oxidized forms) was observed for both **P1** and **P2**.

### Thin-film morphology

Influences of the polymer composition on the thin-film morphology, which can determine the charge-transport properties,

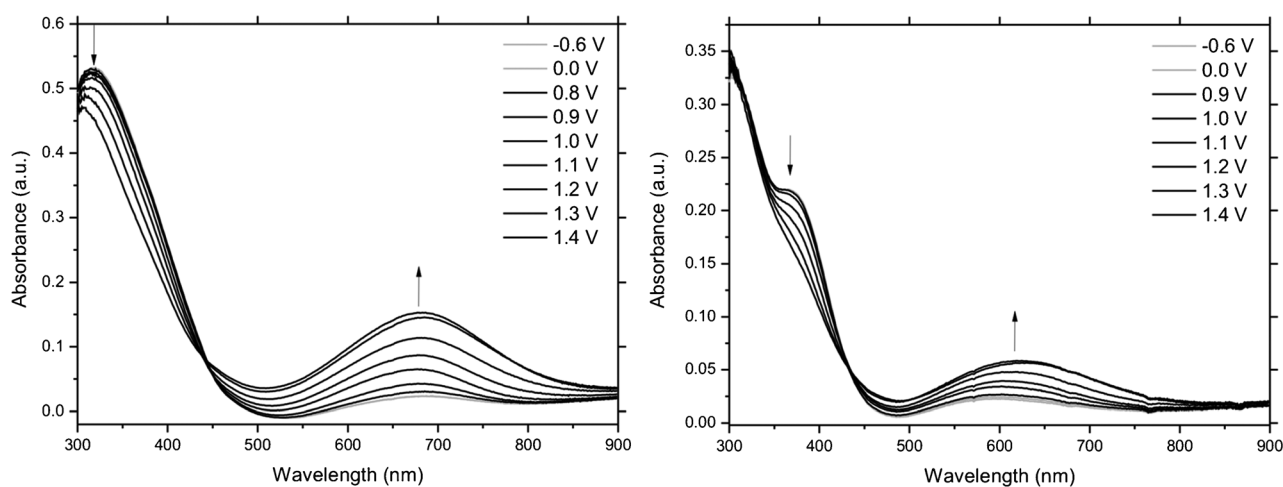


**Figure 4.** UV/Vis spectra recorded during electrochemical oxidation of polymer films **P1** (left) and **P2** (right).

were investigated by atomic force microscopy. Representative AFM images of two anodically polymerized films **P1** and **P2** are shown in Figure S1 of the Supporting Information.

Both materials were obtained from solutions of identical monomer concentration under similar electrochemical conditions. They mask, to some extent, the underlying topography of the polished Pt electrodes. However, their z-color scale bars that represent the overall topography variations differ considerably. For **P1** it corresponds to 100 nm, whereas for **P2** to 800 nm. The root-mean-square (rms) roughness of **P1** (approximately 16 nm over  $100 \mu\text{m}^2$ ) is about 18 times lower than that of **P2** (approximately 286 nm over  $100 \mu\text{m}^2$ ). The difference in the apparent topography of **P1** and **P2** might originate from a number of factors, including the variation in interchain interaction owing to different steric constraints, the variation of the polymerization degree, and hence of the polymer structure. These factors contribute not only to the surface roughness but also to the thickness of the polymer film. As determined by AFM scratching and subsequent imaging, the thickness of **P1** is about 60–90 nm, whereas it is 150–250 nm for **P2**. The difference in thickness might indicate that the formation of the polymer occurs with a simultaneous blocking of the electrode surface in the case of **P1** and with a minor blocking in the case of **P2**. This qualitative behavior is in accordance with the results obtained by impedance spectroscopy.

### Computational study: Structural considerations

The comparison of structural data for dimers of **1** and its analogue substituted with thiophene rings in the 4,5-positions clearly shows that the value of the dihedral angle between the thiophene and xanthenic planes is crucial for the high conductivity achieved owing to close orbital overlapping. Therefore, to minimize steric effects, the heteroaromatic rings were directly attached to the xanthenic moiety in the 2- and 7-positions.

Despite the presence of an  $\text{sp}^3$ -carbon atom (of the  $\text{C}(\text{CH}_3)_2$  group) and oxygen with two single atoms in the central xan-

these ring, the molecular skeleton is planar (Scheme 1). The C–O–C angle of about  $120^\circ$  indicates the involvement of oxygen orbitals in the  $\pi$ -electron conjugation of the molecule (possible  $sp^2$  hybridization). The C–C–C–S dihedral angle between the xanthene and thiophene planes in **P1** amounts to  $28.5^\circ$ , thus indicating the lack of conjugation between these rings. The dimerization of **1** leads to a new C–C bond formed between two thiophene rings. This link only slightly influences the monomeric building blocks. The new structural fragment is characterized by a C–C bond length of  $1.447 \text{ \AA}$  and an S–C–C–S dihedral angle of  $169.5^\circ$ . Further oligomerization (**P1**<sub>n</sub>,  $n=3-5$ ) does not change the C–C–C–S angle and the thiophene–thiophene bonds also remain unchanged. The only variation observed regards the S–C–C–S dihedral angles between thiophene rings, which increase from  $169.5^\circ$  in the dimer to  $177^\circ$  in the pentamer (**P1**<sub>5</sub>). These observations indicate the almost perfect structural additivity of building blocks during the formation of long **P1** oligomers. Ionization leads to a completely planar structure of **1** and **P1**<sub>2</sub>. Complexes **P1**<sub>3</sub> are also planar with the exception of external thiophene rings being slightly twisted by about  $15^\circ$ .

To overcome the low solubility previously noted for many high-molecular-weight semiconducting compounds, alkyl chains were integrated. The modification of **P1** by  $-\text{C}_6\text{H}_{13}$  substitution leads to a significant C–C–C–S angle variation. Its increase to up to  $52^\circ$  indicates the loss of  $\pi$ -electron conjugation. The thiophene–thiophene dihedral angle between subsequent dimers decreases from  $166^\circ$  in the dimer and approaches planarity for **P2**<sub>5</sub>. Other structural parameters remain almost unchanged, which suggests the structural additivity of the **2** building blocks. The effect of the electron loss is significant for short oligomers and results in a more planar structure for the monomer and dimer (C–C–C–S of  $27^\circ$  and S–C–C–S of  $180^\circ$  for the dimer). Owing to charge delocalization the effect starts to disappear for longer oligomers. The main difference between **P1** and **P2** oligomers regards xanthene–thiophene dihedral angles. The decrease in  $\pi$  conjugation owing to the structural perturbation imposed by alkyl chains might have a significant impact on the electronic density organization of the studied moieties. The structural changes influence the theoretical energy-gap value, which is higher for **P2** by  $0.43 \text{ eV}$ .

### The evolution of the molecular orbital space

In monomers the eight highest-occupied molecular orbitals possess  $\pi$  character. The orbitals are delocalized and cover the whole skeleton and include the perpendicular p orbital of the oxygen, C–CH<sub>3</sub> bonds of the xanthene center, as well as single C–C xanthene–thiophene bonds (Figure 5). Six lowest orbitals of the virtual space also possess  $\pi$  character. The orbitals are strongly delocalized, and the  $\pi$  character is not significantly perturbed despite the imperfect planarity of the molecular skeleton. Dimerization results in the formation of a new, formally single C–C bond between the thiophene rings (Scheme 1). This bond, however, is covered by the  $\pi$  orbital localized on the new structural element (Figure 5). This orbital constitutes the highest occupied molecular orbital and belongs to the family of 16 orbitals of  $\pi$  character. The virtual space consists now of 12  $\pi$  orbitals with the LUMO orbital being localized in the area of the newly formed bond. Further extension of the oligomer does not result in qualitative changes. The HOMO/LUMO  $\pi$  space is multiplied, which leads to, for example, 40 (occupied) and 30 (virtual) orbitals in the case of the pentamer and constitutes the base for future polymer bands. Four HOMO and four LUMO orbitals correspond to orbitals of thiophene–thiophene links, and might be considered a building block for valence and conduction bands of **P1**. As expected,

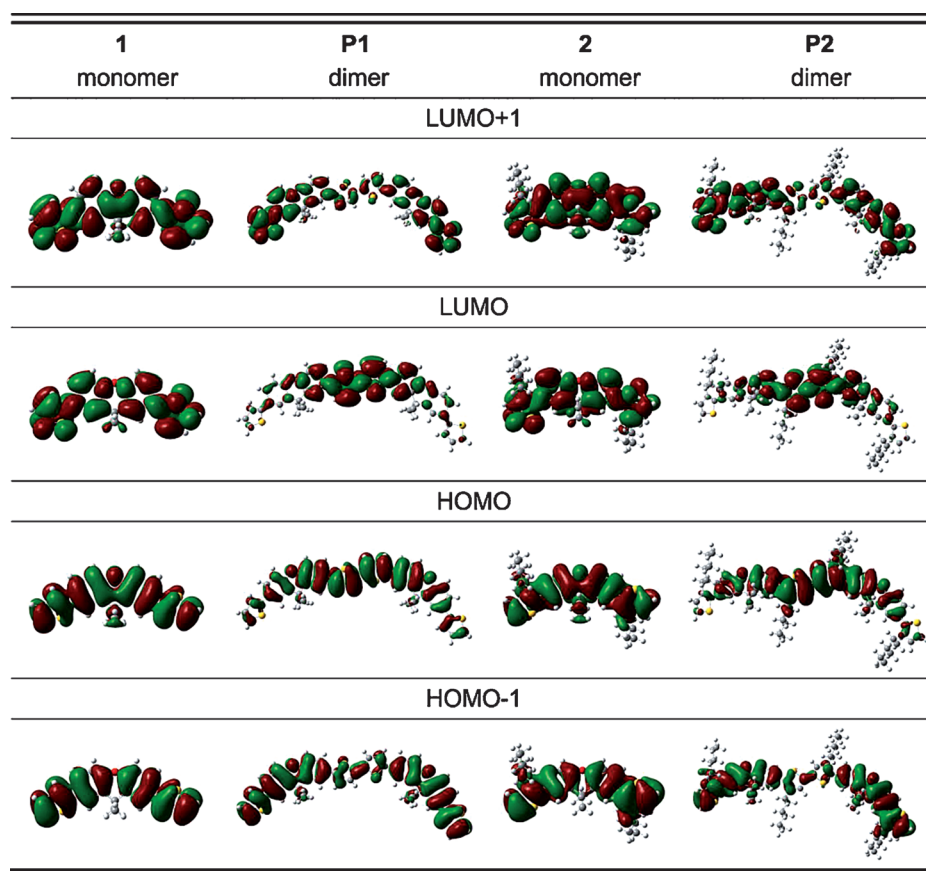
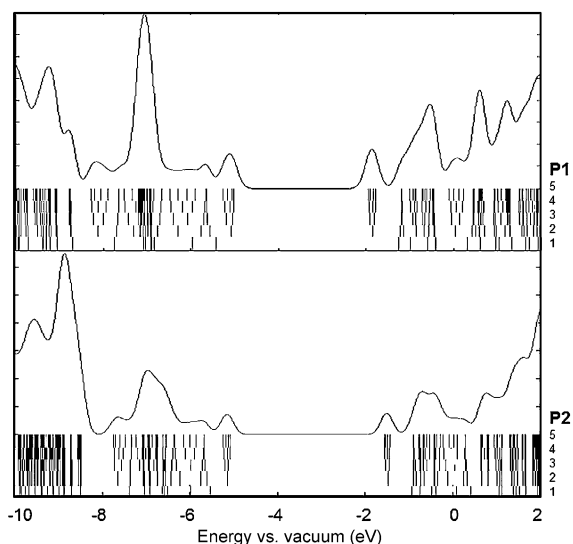


Figure 5. Molecular orbitals obtained from B3LYP/cc-pVDZ studies for the neutral form of **1** and **P1**<sub>2</sub> as well as **2** and **P2**<sub>2</sub>.

the molecular orbital that corresponds to the  $\sigma$  C–C bond is located deep in the orbital space.

Although structural changes occur owing to the attached alkyl chains in the **P2** derivative, the qualitative picture of molecular orbitals (Figure 5) and the variation of energies (Figure 6) are preserved. The extended HOMO/LUMO orbital



**Figure 6.** Plots of density of states for **P1** and **P2** oligomers. The evolution of orbital energy levels is demonstrated below the plots in the order from  $n = 1$  to 5 of the oligomer growth. Energy in eV, intensity in arbitrary units.

space possesses  $\pi$  character and increases by eight occupied and six virtual MOs with each extension of the oligomer by an additional “building” unit. The observation of the space variation for increasing oligomers indicates that the valence and conduction bands are formed from molecular orbitals related to structural fragments between thiophene–xanthene–thiophene blocks.

Despite the fact that the polymerization reaction mechanism is still under debate, it is agreed that it depends on the electron-density distribution. As expected for strongly conjugated molecular systems, the atomic charge as well as electronic spin density are highly delocalized, and the oxidation effect measured by the ionization energy quickly decreases with the extension of the oligomer size. In neutral molecules, charge transfer between xanthene and thiophene units almost does not exist. After ionization every heterocyclic ring shows comparable electron deficiency. The polymerization does not change this picture except for the external rings, which do not lose their electrons in the oxidation process. Those observations confirm an accepted mechanism of the electrochemical polymerization in which the polymer grows by the successive addition of monomers.

Close inspection of natural bond orbital (NBO) atomic charges confirms the additivity of mers in an oligomer. The charge distribution within the mers is almost the same, with an atomic charge on the S atom of 0.413 electrons and of

–0.520 electrons on the O atom. The atomic charge on a carbon atom that takes part in the new C–C bond formation is totally balanced by its neighbor S. This finding indicates the importance of the heteroatom for the polymerization reaction. The electron removal leads to a highly delocalized positive charge distribution with the difference between atomic charges in the cation and parent molecule systematically decreasing as the oligomer grows. The change for the most effected atoms in monomer **1** are 0.054 (S), 0.067 ( $\alpha$ -C), and 0.073 electrons (O) relative to 0.038 (S), 0.023 ( $\alpha$ -C), and 0.026 (O) electrons in its dimer (**P1**<sub>2</sub>). The trend continues when the oligomer grows.

The electron spin density, which represents the  $\alpha$ - and  $\beta$ -electron density difference, is also delocalized (Figure S2 in the Supporting Information). However, the highest concentration of unpaired electrons is found on carbon in the  $\alpha$  position of the external ring, which constitutes a site for polymerization. Since the charge on the carbon in the  $\alpha$  position of the dimer of **2** is slightly lower than the charge localized on its bis-thienyl part, it can meaningfully impair reactivity. The unpaired electron distribution suggests that non-regular linkages might occur. Taking into account the fact that steric effects can influence the polymerization reaction owing to crowding at or near the reactive state, carbon atoms of the bis-thienyl moiety in **P2**<sub>2</sub> in particular are rather inaccessible for the radical cation attack. Moreover, it was previously reported for polythiophene that thienyl rather does not create net structures.<sup>[18]</sup> The stabilization of the radical cation is achieved by the delocalization of the positive charge at longer oligomers, thereby leading to an increased sensitivity towards oxidation processes, which affects further polymerization reactions. The electron density in **P2**<sub>2</sub> is better distributed over the molecule and it will therefore react easily to create longer oligomers. Ionization potentials for both monomers and oligomers (both vertical and adiabatic) are similar with a precision of 0.1 eV; they are 6.7–5.6 eV for vertical and 6.5–5.5 eV for adiabatic.

According to the Koopmans theorem, the HOMO and LUMO orbital energies represent approximately ionization (HOMO) and electron affinity (LUMO) energies. The corresponding experimental values are derived from cyclic voltammetry experiments (see Table 1). The directly calculated DFT values for vertical and adiabatic ionization energies are also reported. Calculations as well as experiments (oxidation energies) indicate a significant change in the ionization energies of the monomer and polymerized materials. The theoretical explanation of this phenomenon is seen in the properties that arose as new C–C bonds formed owing to the polymerization reaction. The most significant change of properties takes place between monomer and dimer, whereas further oligomerization is subject to a slow evolution of properties. The effect is very visible in density-of-states plots (Figure 6) in which the sequence of HOMO and LUMO orbital energies that correspond to the bandgap starts from the dimer molecule. The LUMO orbital energies follow a similar trend with the monomer/dimer energy jump followed by a slow evolution of values. Both experimental and theoretical results indicate the minimal influence of the alkyl chain that modifies **P1**.

## Theoretical absorption spectra

The theoretical absorption spectra were calculated by applying time-dependent density functional theory (TDDFT) (Figure S3 in the Supporting Information). Ten singlet electronic excited states were considered. In the case of **1** the lowest singlet excited state of 332 nm is dominated ( $c=0.701$ ) by the HOMO–LUMO excitation. Dimerization leads to the formation of new HOMO and LUMO orbitals, and the transition between these orbitals constitutes the main component of the lowest singlet excitation in the dimer. The corresponding wave function is dominated by the HOMO–LUMO transition ( $c=0.699$ ) with a significant lowering of the excitation energy of 429 nm. The transition that corresponds to the lowest excitation, which does not involve the thiophene–thiophene link and that corresponds to the HOMO–LUMO orbitals of the monomer are much higher in energy (Figure S3), however, constitutes the second peak of significant intensity. Comparison of the absorption spectra for **P1**<sub>2</sub> and **P2**<sub>2</sub> indicates close qualitative similarities. The differences are quantitative, which leads to energetically lower excitation energies, mainly at 305 nm for the monomer and at 379 nm for the dimer. The second peak of significant intensity corresponds to the HOMO–LUMO transition of the monomer.

The calculated singlet excitation energies, which are the measure of the polymer bandgap, agree reasonably well with the measured UV/Vis spectra. More importantly, calculations provide the qualitative picture of the evolution (Table 1). The measured excitation energy in the monomer and its evolution toward that of the polymer correlates well with the decreasing excitation energy between monomer and dimer. The electrochemical data that represent the valence-conduction bandgaps agree closely with spectroscopic findings as well as with theoretical results. The conductivity of the polymer is controlled by the chemical bonds formed between monomers. The differences between the energy-gap properties of **P1** and **P2** are rather subtle and the comparison should be treated with caution.

## Conclusion

2,7-Dithiophene-substituted xanthene derivatives were synthesized and electrochemically polymerized, thereby leading to the formation of novel p-type organic semiconducting materials. The introduction of a 3-hexyl chain was shown to effectively enhance performance owing to an increase in the porosity of the thin film. Theoretical predictions of the oligomer evolution agree reasonably well with measured data. It was found that the main difference between the single-molecule building block and polymer results from the new C–C bond formed between thiophene rings. This finding indicates the potential of the heteroatom (sulfur) to control the conducting properties of oligomers. The oligomerization has little influence on the structural properties of building blocks. The HOMO/LUMO orbital space indicates significant  $\pi$  conjugation despite the far from perfect planarity and a number of obstacles in the form of

single bonds. The influence of the alkyl chain on chemical properties of oligomers is small.

## Experimental Section

### Materials

2-Thiopheneboronic acid (95%), 3-hexylthiophene-2-boronic acid pinacol ester (95%), tetrakis(triphenylphosphine)palladium(0) (99%), 2-ethoxyethanol (99%), tetrabutylammonium hexafluorophosphate (98%), and potassium hexacyanoferrate(II) trihydrate (98.5%) were purchased from Sigma–Aldrich. Potassium carbonate (99%) was obtained from Chempur. Potassium hexacyanoferrate(III) (99%) was obtained from Honeywell Riedel-de Haën. Acetonitrile (HPLC grade), anhydrous sodium sulfate, and potassium chloride (99%) were purchased from J. T. Baker. Anhydrous magnesium sulfate (98.5%) was received from POCh. All reagents were used without further purification. Preparative column chromatography was performed on glass columns with Fluka silica gel for flash chromatography (mesh 220–440). Aqueous solutions utilized for electrochemical measurements were prepared using Milli-Q water ( $> 18 \text{ M}\Omega \text{ cm}^{-1}$ , Siemens Ultra Pure Water Systems).

### Theoretical methods and computational details

The structures of studied molecules and cations were investigated at the DFT level of theory using a standard cc-pVDZ basis set.<sup>[19]</sup> The B3LYP functional was adopted for these calculations.<sup>[20]</sup> The geometry of oligomers was fully optimized and the minimum-energy structures, in the respective cases, were confirmed through frequency calculations. No symmetry was assumed at the optimization stage of calculations. The singlet and triplet excited-state calculations were performed by applying time-dependent density functional theory (TDDFT).<sup>[21]</sup> Twenty excited electronic states were considered for each molecule. The electron distribution was examined by using NBO and Mulliken electron population analysis schemes.<sup>[22]</sup> The calculations were carried out using Gaussian 09 code.<sup>[23]</sup> The molecular graphics were generated using GaussView 05 and GaussSum software.<sup>[24]</sup>

### Electrochemical and spectroscopic measurements

All electrochemical measurements were recorded with an  $\mu$ Autolab III potentiostat with a frequency response analyzer (FRA) (Metrohm Autolab). Data acquisition and processing were performed using NOVA1.10 software and OriginPro8.1 (OriginLab). The electrochemical cell was comprised of a polycrystalline Pt disc electrode (2.30 mm<sup>2</sup> working area) as a working electrode, an Ag/AgCl/3 M KCl reference electrode, and a platinum coil as auxiliary electrode. The platinum working electrode was polished consecutively with diamond slurries (particle size 3, 1, and 0.5  $\mu\text{m}$ ) on a polishing cloth and afterwards was washed for 15 min in water under sonication. Further cleaning was performed electrochemically by cyclic voltammetry in 0.5 M H<sub>2</sub>SO<sub>4</sub> at a scan rate of 50 mVs<sup>-1</sup> in the potential range between 0.2 and 1.1 V. Polymerization was achieved by cyclic voltammetry (10 cycles) of 0.50 mM monomer solution in acetonitrile at a scan rate of 50 mVs<sup>-1</sup> in the potential range between  $-0.40$  to  $+1.35$  V and  $0.0$  to  $+1.40$  V for **1** and **2**, respectively. As supporting electrolyte, 0.1 M tetrabutylammonium hexafluorophosphate (Bu<sub>4</sub>NPF<sub>6</sub>) was used. Prior to experiments the electrolyte solution was purged with argon and an argon atmosphere was maintained over the solution during the experiment. Electro-

chemical impedance spectra (EIS) were acquired in an equimolar solution (5.0 mM) of  $[\text{Fe}(\text{CN})_6]^{3-/4-}$  at room temperature.

Spectroelectrochemical measurements were performed with a Cary 60 UV/Vis spectrophotometer (Agilent). The potential was controlled with an Autolab PGSTAT101 potentiostat (Metrohm Autolab). Spectra of the polymer films electrodeposited on an indium tin oxide (ITO)-glass electrode were recorded in monomer-free solutions. The same supporting electrolyte as the one used for polymerization was employed. ITO-glass electrodes were degreased by means of sonication in acetone for 30 min and boiling in 0.1 M sodium hydroxide before polymer deposition. The background absorption was measured in a cell with a bare ITO electrode. For both polymer films the UV/Vis spectra were determined in a potential range between -0.4 and 1.4 V with the 0.1 V steps. At each applied potential, the quasi-equilibrium was allowed to be reached before the spectra were recorded.

$^1\text{H}$  and  $^{13}\text{C}$  NMR spectra were recorded in deuterated chloroform  $\text{CDCl}_3$  with a Bruker DRX 300 Avance Instrument. Chemical shifts in ppm ( $\delta$ ) were referenced to the residual solvent signal. Elemental analysis was performed with an Elementar Vario EL III. Topographical and morphological information was obtained with a JPK Nanoscope 3 atomic force microscope equipped with a Vortis controller. Tapping mode was used for AFM imaging in air. Contact mode was used for lithographical scratching of polymer films.

## Synthesis

**2,7-Bis(thiophen-2-yl)-9,9-dimethylxanthene (1):** 9,9-Dimethylxanthene (**3**) was prepared according to a procedure reported in the literature.<sup>[25]</sup> 2,7-Dibromo-9,9-dimethylxanthene (**4**) was obtained by following the method proposed by D. J. Adams et al.<sup>[26]</sup> 2,7-Bis(thiophen-2-yl)-9,9-dimethylxanthene (**1**) was synthesized by analogy with a procedure previously developed by Hemgesberg and co-workers.<sup>[10]</sup> In a three-necked round-bottomed flask 2,7-dibromo-9,9-dimethylxanthene (**4**) (1.84 g, 5.00 mmol) and 2-thiopheneboronic acid (1.41 g, 11.00 mmol) were dissolved in 2-ethoxyethanol (45 mL). Potassium carbonate (3.04 g, 0.02 mol) dissolved in distilled water (5 mL) was added, followed by 0.4 mol% tetrakis(triphenylphosphine)palladium(0) (0.023 g, 0.02 mmol). The reaction mixture was heated for 24 h at 130 °C under nitrogen. After cooling to room temperature, the mixture was diluted with water and extracted with chloroform. The solvent was removed under vacuum, and the residue was purified by means of column chromatography (hexane/chloroform). Crystallization from benzene gave greenish crystals of **1** (0.78 g, 42%).

$^1\text{H}$  NMR (300 MHz,  $\text{CDCl}_3$ ):  $\delta$  = 1.72 (s, 6H;  $\text{CH}_3$ ), 7.11–7.04 (m, 4H; Ar–H), 7.26 (d,  $^3J$  = 4.3 Hz, 4H; Ar–H), 7.46 (dd,  $^3J$  = 8.4 Hz,  $^4J$  = 2.2 Hz, 2H; Ar–H), 7.64 ppm (d,  $^4J$  = 2.2 Hz, 2H; Ar–H);  $^{13}\text{C}$  NMR (75 MHz,  $\text{CDCl}_3$ ):  $\delta$  = 32.7, 34.2, 117.0, 122.6, 124.0, 124.3, 125.5, 128.1, 129.8, 130.2, 144.3, 149.8 ppm; elemental analysis calcd (%) for  $\text{C}_{23}\text{H}_{18}\text{OS}_2$ : C 73.76, H 4.84, S 17.12; found: C 73.89, H 5.15, S 17.26.

**2,7-Bis(3-hexylthiophen-2-yl)-9,9-dimethylxanthene (2):** The synthesis of monomer **2** was adapted from the procedure that was utilized for its analogue **1**. 2,7-Dibromo-9,9-dimethylxanthene (**4**) (2.84 g, 7.72 mmol), 3-hexylthiophene-2-boronic acid pinacol ester (5.0 g, 16.99 mmol), potassium carbonate (4.70 g, 33.97 mol), and 0.4 mol%  $[\text{Pd}(\text{PPh}_3)_4]$  (0.031 g, 0.036 mmol) in a solution of 2-ethoxyethanol/water (9:1, 80 mL) were heated together at 130 °C under an inert nitrogen atmosphere for 48 h. After cooling to room temperature, the mixture was diluted with water and extracted with

chloroform. The crude product was purified by means of column chromatography (hexane/chloroform) and gave a light green oil of **2** (1.30 g, 31%).

$^1\text{H}$  NMR (300 MHz,  $\text{CDCl}_3$ ):  $\delta$  = 0.90 (t,  $^3J$  = 6.7 Hz, 6H;  $\text{CH}_3$ ), 1.43–1.26 (m, 12H;  $\text{CH}_2$ ), 1.73–1.61 (m, 4H;  $\text{CH}_2$ ), 1.74 (s, 6H;  $\text{CH}_3$ ), 2.75–2.63 (m, 4H;  $\text{CH}_2$ ), 7.02 (d,  $^3J$  = 5.2 Hz, 2H; Ar–H), 7.15 (d,  $^3J$  = 8.4 Hz, 2H; Ar–H), 7.25 (d,  $^3J$  = 5.2 Hz, 2H; Ar–H), 7.32 (dd,  $^3J$  = 8.4 Hz,  $^4J$  = 2.1 Hz, 2H; Ar–H), 7.53 ppm (d,  $^4J$  = 2.1 Hz, 2H; Ar–H);  $^{13}\text{C}$  NMR (75 MHz,  $\text{CDCl}_3$ ):  $\delta$  = 14.2, 22.8, 28.9, 29.4, 31.3, 31.8, 32.6, 34.3, 116.6, 123.4, 127.5, 128.7, 129.6, 129.8, 137.8, 138.6, 149.8 ppm; elemental analysis calcd (%) for  $\text{C}_{35}\text{H}_{42}\text{OS}_2$ : C 77.44, H 7.80; S 11.81; found: C 77.69, H 8.08, S 11.32.

## Acknowledgements

The Polish National Centre of Progress of Explorations (grant no. 2012/05/B/ST5/00749) and the Wrocław University of Technology are gratefully acknowledged. K.O. thanks the German Academic Exchange Service (DAAD) and the European Union as part of the European Social Fund for a financial scholarship. The Wrocław Centre of Computing and Networking is acknowledged for generous allotments of computer time.

**Keywords:** conducting materials • density functional calculations • electrochromic effect • polymers • xanthene

- [1] a) J. Roncali, *Annu. Rep. Prog. Chem. Sect. C: Phys. Chem.* **1999**, *95*, 47–88; b) C. Liao, F. Yan, *Polym. Rev.* **2013**, *53*, 352–406.
- [2] Y. Shirota, *J. Mater. Chem.* **2000**, *10*, 1–25.
- [3] a) R. D. McCullough, S. P. Williams, *J. Am. Chem. Soc.* **1993**, *115*, 11608–11609; b) R. E. Martin, F. Diederich, *Angew. Chem. Int. Ed.* **1999**, *38*, 1350–1377; *Angew. Chem.* **1999**, *111*, 1440–1469.
- [4] J. Kim, K. J. Baeg, D. Khim, D. T. James, J. S. Kim, B. Lim, J. M. Yun, H. G. Jeong, P. S. K. Amegadze, *Chem. Mater.* **2013**, *25*, 1572–1583.
- [5] a) G. Gomez-Sosa, M. F. Beristain, A. Ortega, J. Martinez-Viramontes, T. Ogawa, R. C. Fernandez-Hernandez, L. Tamayo-Rivera, J. A. Reyes-Esqueda, T. Isoshima, M. Hara, *Opt. Mater.* **2012**, *34*, 856–860; b) J. Dong, M. Wang, P. Zhang, S. Yang, J. Liu, X. Li, L. Sun, *J. Phys. Chem. C* **2011**, *115*, 15089–15096; c) G. D. Sharma, P. Balraju, M. Kumar, M. S. Roy, *Mater. Sci. Eng. B* **2009**, *162*, 32–39.
- [6] a) Z. Chu, D. Wang, C. Zhang, F. Wang, H. Wu, Z. Lv, S. Hou, X. Fan, D. Zou, *Synth. Met.* **2012**, *162*, 614–620; b) S. J. Zhang, Q. Q. Bu, Y. F. Li, C. L. Gong, X. Y. Xu, H. Li, *Mater. Chem. Phys.* **2011**, *128*, 392–399.
- [7] Z. N. Tisseh, S. C. Azimi, P. Mirzaei, A. Bazgir, *Dyes Pigm.* **2008**, *79*, 273–275.
- [8] Y. Morisaki, J. A. Fernandes, Y. Chujo, *Macromol. Chem. Phys.* **2010**, *211*, 2407–2415.
- [9] K. M. Lefler, K. E. Brown, W. A. Salamant, S. M. Dyar, K. E. Knowles, M. R. Wasielewski, *J. Phys. Chem. A* **2013**, *117*, 10333–10345.
- [10] M. Hemgesberg, D. M. Ohlmann, Y. Schmitt, M. R. Wolfe, M. K. Müller, B. Erb, Y. Sun, L. J. Gooßen, M. Gerhard, W. R. Thiel, *Eur. J. Org. Chem.* **2012**, 2142–2151.
- [11] F. Bellina, A. Carpita, R. Rossi, *Synthesis* **2004**, 2419–2440.
- [12] M. Łapkowski, P. Data, A. Nowakowska-Oleksy, J. Słoduch, S. Roszak, *Mater. Chem. Phys.* **2012**, *131*, 757–763.
- [13] G. Inzelt in *Conducting Polymers: A new Era in Electrochemistry* (Eds.: F. Scholz), Springer, Berlin, Germany, **2008**, pp. 68–87.
- [14] M. E. G. Lyons in *Electroactive Polymer Electrochemistry Part 1: Fundamentals* (Eds.: M. E. G. Lyons), Springer, New York, USA, **2010**, pp. 6–120.
- [15] M. Bledowski, L. Wang, A. Ramakrishnan, O. V. Khavryuchenko, V. D. Khavryuchenko, C. Ricci, J. Strunk, T. Cremer, C. Kolbeck, R. Beranek, *Phys. Chem. Chem. Phys.* **2011**, *13*, 21511–21519.
- [16] A. Moliton, R. C. Hiorns, *Polym. Int.* **2004**, *53*, 1397–1412.

- [17] A. O. Patil, A. J. Heeger, F. Wudl, *Chem. Rev.* **1988**, *88*, 183–200.
- [18] R. J. Waltman, J. Bargon, *Can. J. Chem.* **1986**, *64*, 76–95.
- [19] T. H. Dunning, *J. Chem. Phys.* **1989**, *90*, 1007–1023.
- [20] a) A. D. Becke, *J. Chem. Phys.* **1993**, *98*, 5648–5652; b) S. H. Vosko, L. Wilk, M. Nusair, *Can. J. Phys.* **1980**, *58*, 1200–1211; c) C. Lee, W. Yang, R. G. Parr, *Phys. Rev. B* **1988**, *37*, 785–789.
- [21] a) R. E. Stratmann, G. E. Scuseria, M. J. Frisch, *J. Phys. Chem.* **1998**, *109*, 8218–8224; b) M. E. Casida, C. Jamorski, K. C. Casida, D. R. Salahub, *J. Chem. Phys.* **1998**, *108*, 4439–4449.
- [22] F. Weinhold, J. E. Carpenter in *The Structure of Small Molecules and Ions* (Eds.: R. Naaman, Z. Vager), Plenum Press, New York, USA, **1988**, pp. 227–236.
- [23] Gaussian 09, Revision D.01, M. J. Frisch, G. W. Trucks, H. B. Schlegel, G. E. Scuseria, M. A. Robb, J. R. Cheeseman, G. Scalmani, V. Barone, B. Men-  
nucci, G. A. Petersson, H. Nakatsuji, M. Caricato, X. Li, H. P. Hratchian,  
A. F. Izmaylov, J. Bloino, G. Zheng, J. L. Sonnenberg, M. Hada, M. Ehara,  
K. Toyota, R. Fukuda, J. Hasegawa, M. Ishida, T. Nakajima, Y. Honda, O.  
Kitao, H. Nakai, T. Vreven, J. A. Montgomery, Jr., J. E. Peralta, F. Ogliaro,  
M. Bearpark, J. J. Heyd, E. Brothers, K. N. Kudin, V. N. Staroverov, R. Ko-  
bayashi, J. Normand, K. Raghavachari, A. Rendell, J. C. Burant, S. S. Iyen-  
gar, J. Tomasi, M. Cossi, N. Rega, J. M. Millam, M. Klene, J. E. Knox, J. B.  
Cross, V. Bakken, C. Adamo, J. Jaramillo, R. Gomperts, R. E. Stratmann,  
O. Yazyev, A. J. Austin, R. Cammi, C. Pomelli, J. W. Ochterski, R. L. Martin,  
K. Morokuma, V. G. Zakrzewski, G. A. Voth, P. Salvador, J. J. Dannenberg,  
S. Dapprich, A. D. Daniels, Ö. Farkas, J. B. Foresman, J. V. Ortiz, J. Cio-  
slowski, D. J. Fox, Gaussian, Inc., Wallingford CT, USA **2009**.
- [24] a) GaussView, Version 5, R. Dennington, T. Keith, J. Millam, Semichem  
Inc., Shawnee Mission, KS, USA, **2009**; b) N. M. O'boyle, A. L. Tenderholt,  
K. M. Langner, *J. Comput. Chem.* **2008**, *29*, 839–845.
- [25] J. S. Nowick, P. Ballester, F. Ebmeyer, J. Rebek, *J. Am. Chem. Soc.* **1990**,  
*112*, 8902–8906.
- [26] D. J. Adams, D. J. Cole-Hamilton, D. A. J. Harding, E. G. Hope, P. Pogorze-  
lec, A. M. Stuart, *Tetrahedron* **2004**, *60*, 4079–4085.

---

Received: October 12, 2014

Revised: December 16, 2014

Published online on January 14, 2015